AIAA JOURNAL
Vol. 48, No. 3, March 2010

Adaptive Snubber-Type Magnetorheological Fluid–Elastomeric Helicopter Lag Damper

Grum T. Ngatu,* Wei Hu,† and Norman M. Wereley‡
University of Maryland, College Park, Maryland, 20740
and
Curt S. Kothera§
Techno-Sciences, Inc., Beltsville, Maryland, 20705

DOI: 10.2514/1.43356

A snubber-type magnetorheological fluid–elastomeric lag damper is developed to provide adaptive lead-lag damping augmentation for a hingeless helicopter rotor. The magnetorheological fluid–elastomeric lag damper consists of a flow valve, a flexible snubber body, and a flexible center wall separating the body into two fluid chambers. Magnetorheological fluid enclosed in the snubber body can flow through two magnetorheological valves and be activated by a magnetic field in the valves. Consistent with the loading conditions for a helicopter lag damper, the magnetorheological fluid–elastomeric damper is tested under single and dual frequency excitations. The complex modulus method was used to compare the magnetorheological fluid–elastomeric device damping performance with the baseline passive Fluidlastic damper. A significant controllable damping range is observed as current is applied to the magnetorheological valve in the magnetorheological fluid–elastomeric damper. Furthermore, to account for the nonlinear hysteresis behavior of the magnetorheological fluid–elastomeric damper and estimate the damping force, a time-domain hydromechanical model is formulated based on lumped parameters. Model parameters are established using damper geometry, material properties, and experimental data. The model is then applied to simulate the force vs displacement response and force time history under both single and dual frequency excitations.

Nomenclature

A	=	area
A_d	=	active gap area
A_p	=	effective pressure area
C_c	=	bulge damping
C_{eq}	=	equivalent viscous damping
C_r	=	shear damping
D	=	diameter
D_o	=	flux-return outer diameter
d	=	active gap thickness
E	=	error function
F	=	force
F_{MR}	=	MR valve force
F^*	=	model estimated force
F_c	=	first cosine force Fourier coefficient
F_s	=	first sine force Fourier coefficient
F_y	=	yield force
H	=	magnetic field
I	=	inertance
k_c	=	bulge stiffness
k_r	=	shear stiffness
k^*	=	complex modulus
k'	=	in-phase stiffness
k''	=	loss stiffness
L_c	=	active valve length
L_p	=	passive valve length
l	=	length
m	=	mass
m_r	=	elastomer mass
P	=	pressure
q	=	flow rate
R	=	resistance
r	=	bobbin radius
S	=	compliance
t	=	time
X_c	=	first cosine displacement Fourier coefficient
X_s	=	first sine displacement Fourier coefficient
X_{lag}	=	input amplitude at lag/rev frequency
X_{pri}	=	input amplitude at 1/rev frequency
x	=	input displacement
x_a, x_b	=	inertance displacements
x_A, x_B	=	generalized inertance displacements
A, B	=	generalized valve index
a, b	=	valve index
i	=	control volume index
j	=	sampling index
ΔP	=	pressure drop over MR valve
η	=	loss factor
μ_o	=	MR fluid viscosity
μ_{MR}	=	postyield MR fluid viscosity
ρ	=	MR fluid density
τ_y	=	yield shear stress
ψ	=	valve factor
ω	=	frequency
$\%\mathrm{Vol}_{\mathrm{MR}}$	=	fraction of total displaced fluid volume flowing through MR valve

Received 21 January 2009; revision received 30 October 2009; accepted for publication 3 November 2009. Copyright © 2009 by Norman M. Wereley. Published by the American Institute of Aeronautics and Astronautics, Inc., with permission. Copies of this paper may be made for personal or internal use, on condition that the copier pay the $10.00 per-copy fee to the Copyright Clearance Center, Inc., 222 Rosewood Drive, Danvers, MA 01923; include the code 0001-1452/10 and $10.00 in correspondence with the CCC.

*Graduate Research Assistant; grum@umd.edu. Sloan Fellow. Student Member AIAA, AHS, ASME, and NSBE.

†Assistant Research Scientist; weihu@umd.edu. Member AIAA and AHS.

‡Professor; wereley@umd.edu. Associate Fellow AIAA. Fellow IOP and ASME.

§Research Engineer; kotherac@technosci.com. Member ASME and AHS. Senior Member AIAA.

I. Introduction

MOST modern soft-in-plane helicopter main rotors are equipped with lead-lag dampers to alleviate aeromechanical instabilities such as air and ground resonance resulting from the interaction of the poorly damped regressing lag mode of the rotor blades with the body support modes [1]. These types of rotors are typically fitted with lag dampers made of passive materials, such as elastomers, to dissipate

energy [2–5]. Compared with conventional hydraulic lag dampers, elastomeric lag dampers have a lower parts count and are lighter in weight, easier to maintain, and more reliable [4,6]. Unlike hydraulic dampers, elastomeric dampers do not produce extremely high damping forces at high lead-lag velocities [6]. To provide the required damping, a highly hysteretic elastomeric material is used. Under dynamic lag motions, the elastomer is sheared and provides damping through energy dissipation. In addition, the elastomer introduces stiffness into the system, which can be used as a design parameter to change the natural frequency of the lag mode to avoid resonances [6,7]. However, these highly damped elastomers exhibit a nonlinear hysteretic response to dynamic loading. Furthermore, the damping and stiffness properties of elastomeric dampers are nonlinear functions of lag frequency, dynamic lag amplitude, and operating temperature. It has been shown that elastomeric damping and stiffness levels diminish markedly as amplitude of damper motion increases [2–7]. In addition, there is a reduction in damping as the excitation frequency is increased. At small lead-lag displacements, these elastomeric dampers have exhibited low loss factors and high stiffness, resulting in unfavorable limit-cycle instabilities [4]. In forward-flight conditions, the blade lead-lag motion in helicopters occurs at two frequencies, the lead-lag frequency and 1/rev frequency, and as the 1/rev amplitude is increased, it substantially reduces damping at lower lag/rev amplitudes, thus causing undesirable limit-cycle oscillations [4,6]. To address these undesirable effects of elastomeric dampers, a hybrid viscous fluid and elastomeric damper, referred to as a Fluidlastic lag damper, was uniquely designed by Lord Corporation [2,4,8,9]. These fluid–elastomeric or Fluidlastic lag dampers alleviate the undesirable effects of nonlinear elastomeric dampers behavior by minimizing the dependence of the lag-mode damping and stiffness on amplitude and frequency, resulting in a predominantly linear performance. Since the majority of damping is supplied through viscous damping, the elastomeric material employed need not be selected based on its damping property, but rather on its stiffness and shear fatigue properties [8]. Even though Fluidlastic lag dampers provide a substantially improved performance over elastomeric dampers, they are limited to providing fixed or passive damping. Since damping augmentation is only required over certain flight regimes where there is a potential for instabilities to occur [10], a passive damper providing a fixed damping could produce unfavorably large periodic loads on the rotor hub. Furthermore, passive dampers tend to present damping loss as temperature increases either due to in-service self-heating or hot operating conditions. Under these circumstances, elastomer softening and/or fluid thinning occurs, which adversely affects damper performance [2–4,11,12]. Thus, an adaptive damper, which can produce the desired amount of damping without a corresponding increase in periodic loads and can be adjusted to compensate for performance losses at extreme environmental conditions, would be of considerable value.

Magnetorheological (MR) fluids typically consist of spherical micron-sized magnetic particles (microspheres) suspended in a liquid medium such as silicone or hydraulic oil [13,14]. Their rheological properties, that is their yield stress and viscosity, can be rapidly and continuously controlled by varying the applied magnetic field. Conventional MR fluids use spherical micron-sized iron particles at high weight fractions and have been shown to exhibit high yield stresses, up to 100 kPa [15,16]. The fast response and controllability of MR fluids are advantageous for implementation in semi-active smart vibration-absorption systems [17], primary vehicle suspension systems [18,19], landing gear for aircraft [20–22], adaptive crew seats for vibration [23–25], and shock isolation [26,27]. Because the yield stress of the MR fluid exhibits a substantial controllable range when a magnetic field is applied, many MR fluid-based devices were designed such that the damping level can be controlled in feedback by applying a magnetic field [28,29]. MR fluids have also been considered for application to helicopter rotorlag dampers [7,10,30,31]. Much of this work has been done to evaluate the feasibility and capabilities of employing MR dampers in conjunction with elastomeric materials in helicopter lead-lag damping applications. Kamath et al. [10,31] modified a pair of 1/6th-Froude-scale Comanche helicopter fluid–elastomeric lag dampers to a pair of hybrid elastomeric MR dampers and demonstrated their capability for lag-mode damping applications. Hu and Wereley [7] also conducted analytical and experimental studies on a parallel arrangement of an elastomeric lag damper and two conventional MR dampers, and demonstrated a significant controllable-damping dynamic range. Recently, a full-scale linear-stroke tubular magnetorheological fluid–elastomeric (MRFE) lag damper, which can be fully integrated into an actual helicopter rotor system, was developed [30]. The linear-stroke MRFE lag damper was developed as a retrofit to an existing elastomeric lag damper, configured to shear elastomeric material sandwiched between two concentric tubes, which move relative to each other. In the inner metallic tube of the elastomeric damper, a piston, an MR valve, and MR fluid were introduced. In this arrangement, the elastomeric and MR damping effects are decoupled systems, such that their individual contribution can be nearly superposed to yield the total MRFE damper performance. In this study, it was shown that in the field-off-condition, the MRFE damper behaves like an elastomeric damper. As magnetic field is applied, the damping of the MRFE device can be varied substantially and, thus, has the potential to augment damping over critical frequency range of the helicopter rotor.

In the present study, a full-scale MRFE lag damper is developed by incorporating two MR valves into a snubber-type round-stacked Fluidlastic lead-lag damper. The device was experimentally evaluated for its controllable damping capability and dynamic range under sinusoidal excitation, consistent with helicopter lead-lag-damper loading conditions. Because of kinematical complexity in modern hingeless helicopter main rotors, a snubber-type lag damper is usually made from a laminated stack of alternating elastomeric–metallic rings, and damping fluids are included in the flexible body to increase dynamic range of the snubber damper [32]. In the present Fluidlastic lag damper, a multiple lamination of elastomeric and metallic rings forms the cylindrical damper body with two chambers. The flexing of the elastomeric container forces fluid to flow from one chamber into the other through flow ports, thus providing the required damping. This Fluidlastic damper has an advantage over conventional linear-stroke hydraulic dampers, as it does not include any moving parts, thus avoiding the issue of wear and leakage. Although the elastomer introduces a significant stiffness to the system, its damping contribution is minimal compared with the viscous damping generated. The MRFE damper uses the existing flexible damper body and the flexible center wall of the Fluidlastic damper (also referred to as the baseline damper), with the two port holes in the center wall retrofitted with one MR valve each. The MRFE damper can provide controllable damping and can potentially augment damping over critical frequency ranges and adverse operating conditions and can increase stability of a helicopter rotor. Further, the MRFE damping components can still provide fail-safe passive damping in the event of reduced or no-power operation. The MRFE retrofit shares a similarity with the baseline damper as it does not introduce any moving component.

The complex modulus method is employed to characterize the MRFE damper performance and to compare it with the baseline damper. It is shown that the field-off damping of the MRFE damper is less than the baseline snubber damper, and a significant damping control range, extending beyond the baseline damper, can be provided by the MRFE damper with the application of an increasing magnetic field. However, the complex modulus linearization technique does not identify and describe the nonlinear behavior of the MRFE damper under sinusoidal excitation, which is a consequence of the magnetorheological effect. Various models based on lumped parameter approaches have been proposed to model the nonlinear hysteretic behavior of elastomeric lag dampers [3,5,33–35], MR dampers [10,31,36–40], and hybrid elastomeric–MR and MRFE lag dampers [7,10,30,31] under harmonic excitations. In an elastomeric material, where nonlinear behaviors arise from excitation amplitude, frequency, and temperature, the complex modulus can be computed at each test condition to reconstruct the hysteretic characteristics with an acceptable accuracy. However, most elastomeric lag dampers are filled elastomers and exhibit hysteretic behavior that is also displacement- and velocity-dependent, resulting in a nonelliptical shear strain vs shear stress curve when undergoing harmonic

excitation. In this regard, Grilli et al. [3] proposed a nonlinear model that combines a Kelvin chain in parallel with a cubic spring and a linear elasto-slide element. Hu and Wereley [5] developed a model based on the triboelastic theory, which combined rate-dependent elasto-slide elements with a yield-distribution function to account for the yield force. Classic Bingham-plastic- and Herschel–Bulkley-based models have been used to model ER and MR devices [36–38]. Further, mechanism- and/or physically-motivated models have been developed to characterize MR dampers. Kamath et al. [10,31] presented a hysteretic model combining a stiffness plus viscoelastic–plastic model with a nonlinear weighting function. Hu and Wereley formulated the rate-dependent elasto-slide model, which uses a rate-dependent slide and a parallel viscous damper to emulate the yield behavior of the MR fluid, and uses a stiff spring in series to represent the preyield behavior [40]. These models were able to capture and reconstruct the nonlinear dynamic-hysteresis behavior of elastomeric and MR dampers for the tested amplitude and frequency spectrum. All these parametric models are based on the physical phenomena of the system whereby a series of mechanisms are lumped to relate the input to the output. However, these models do not describe the actual physical-flow phenomena or flow dynamics in fluid-based MR dampers. They do not show the interaction between mechanical and hydraulic systems, which is an inherent feature of hydraulic-based MRFE dampers. Thus, a hydromechanical model, which can delineate the physical flow motion of the system and accurately describe the nonlinear hysteretic behavior of the MRFE damper, is proposed. Although hydromechanical modeling has been applied in passive systems [41,42] and active ER and MR damper systems [43,44], there only have been limited studies in their application in helicopter damping systems and specifically in snubber-type MRFE lag dampers, which are coupled systems of MR fluid and elastomeric material. The hydromechanical model explored in this study is a design-based model which describes the damper system with a series of lumped hydraulic and mechanical components. The model employs physical parameters such as inertia, damping, yield force, and compliances, which are dependent on damper geometry and material properties of components and which can potentially be approximated a priori. Previous MRFE dampers have decoupled systems, which are basically modeled as a parallel combination of elastomeric and MR damper elements [7,30]. In the current MRFE lag damper, the hydromechanical model is able to account for the coupling between the elastomeric material and the MR system, which is manifested through chamber compliances. Once model parameters have been established, the model is shown to simulate accurately the measured hysteretic force-displacement history under single and dual frequency excitations.

II. Development of MRFE damper

A section view of the baseline Fluidlastic damper is shown in Fig. 1. The flexible body of the damper is made of metallic shims interspersed with elastomeric layers, or a multiple lamination of metallic and elastomeric ring layers. These laminates are bonded to metallic plates at both ends. At center height, a circumferential middle plate is attached to the elastomeric cylinder wall. This flexible center wall is placed in the middle of the cavity of the snubber body to divide the cavity into two fluid chambers. A flexible center wall made of rubber runs along the diameter of the flexible cylinder, completely molded at both ends to the elastomeric damper body. This creates two distinct volume chambers into which a viscous fluid is poured and completely sealed. The only way the two chambers communicate is through two flow ports, which are incorporated in the center wall. There are four threaded holes for filling and draining fluid, two on each side of the damper. Once fluid is injected into the chambers, the holes are bolted and a compression bolt is mounted through the vertical center hole of the damper assembly, which creates a positive internal pressure. This damper has a compact size with a height of about 4.20 in and diameter of 4.65 in. In the current helicopter rotor system as shown in Fig. 2, each blade is equipped with a pair of Fluidlastic lag dampers. The lag dampers, which are housed in the pitch-horn-adapter assembly, are attached to the inboard side of the blade cuff or torque tube, which in turn is attached to the blade and flexure at its outboard end. The paired lag dampers are interconnected by a shear restraint, which is installed in the composite yoke flexure. The relative motion of the flexure yoke and the torque tube, which constitutes the lead-lag motion, deforms the paired lag dampers. The flow ports are located in the middle of the flexible center wall, and the deformation of the snubber body can force the fluid to flow between chambers through these port holes, providing the required blade lead-lag damping.

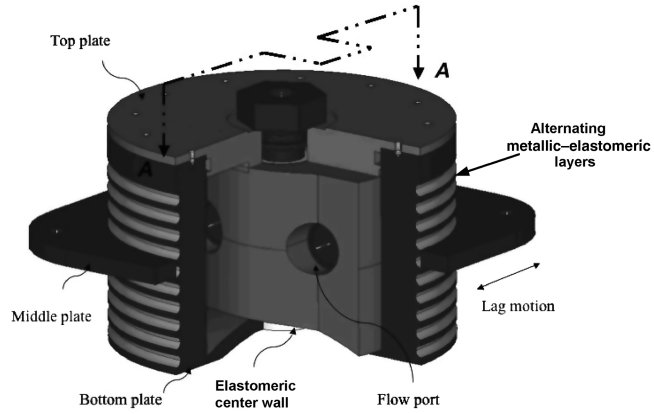

Fig. 1 Partially sectioned isometric view of Fluidlastic lag damper.

The design of the MRFE damper requires the development and retrofit of two MR valves inside the existing baseline damper body and exchange of the existing passive, hydraulic fluid with field-controllable, MR fluid (provided by LORD Corp.). The development of the MR valves involves fitting the existing two port holes located in the center wall with two flow-mode MR valves. The development of the MR valves inside the existing lag-damper center wall is shown in Fig. 3. These internal MR valves are placed at the two existing flow ports, located in the center wall, one per hole on either side of the fluid chambers. Figure 3a shows the top view (top plate removed) of the lag damper with MR valves installed. The new MR retrofit design introduces only the MR valves. Thus, the MRFE still maintains the durability and leakage-free feature of the baseline damper. In addition, this helps minimize the weight penalty incurred due to addition of components. Figure 3b shows a detailed sketch of one of the incorporated MR valves with its basic components. The MR valve includes a bobbin with coil and a flux return, which in this case is designed in the shape of a stepped hollow cylinder, with the wider portion accommodating the bobbin and a smaller one to be threaded into the flow ports. The diameter of the flow port has been oversized as much as possible to reduce associated viscous losses. Magnetic field is provided by an electromagnet enclosed in the valve such that the MR fluid flowing through the flow valve can be activated. The top plate of the original damper has also been modified to have access to the enclosed electromagnet's wires to apply current.

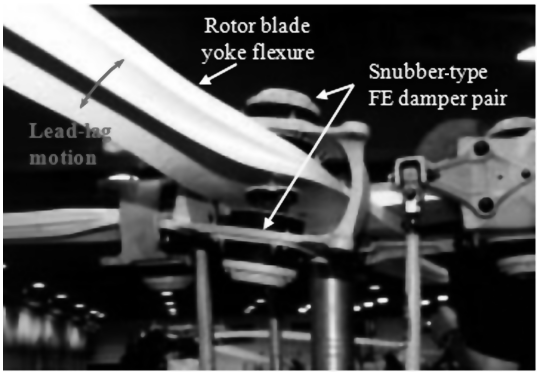

Fig. 2 Schematic of main rotor blade with paired FE lag dampers (Courtesy of Bell Helicopter).

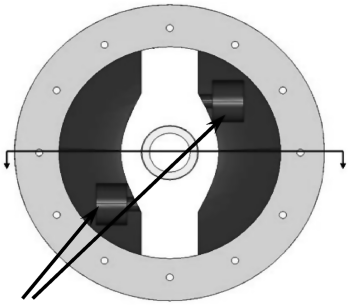

a) Damper top view

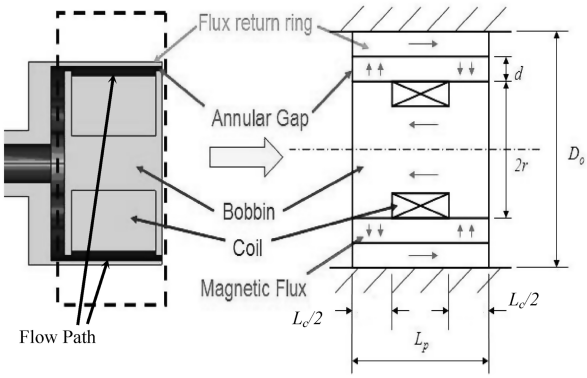

b) MR valve details

Fig. 3 MRFE damper design details.

Figure 3b also shows the flow path of the MR fluid in the valve. The damper is assembled as a sealed unit, so that minimal possibility exists for the fluid to pass from one chamber to the other without traveling through the flow port of the MR valve. The electromagnetic coil in the MR valve is wound around the bobbin, which is inserted into the flux return. The annular gap thickness can be varied by changing the radius of the bobbin r, changing the inner diameter of the flux-return ring, or changing both at the same time. The active valve length L_c can be adjusted to increase or decrease the magnetic flux that activates the MR fluid as well. Overall, the maximum size of the valve, specified by the flux return outer diameter D_o and the valve length L_p, determines whether the valve fits within the constraints of the existing damper body and does not affect the required stroke of the damper to avoid contact with the outer cylindrical wall, which are the goals of the design. Figure 3b also depicts the path of the magnetic flux, which is initiated upon application of a current. In addition to imposing constraints on valve sizing, the current MR retrofit package creates unfavorable passive viscous losses due to unavoidable fluid flow through small-diameter passageways and 90° turns, resulting from the existing Fluidlastic lag-damper design feature. Future designs can avoid these unfavorable conditions by designing an MR retrofit that can be fully embedded in the center wall of the baseline damper. The original baseline damper is preloaded in compression, and the viscous fluid inside the chambers is sealed under pressure. However, during assembly of the prototype parts, the MR fluid was injected under no pressure and the elastomer was approximately 18% precompressed, which is less than the roughly 20% precompression of the baseline damper.

III. Linearized damper performance evaluation

To evaluate the MR valves, the baseline damper dynamics were first studied. For small displacement applied at the center of the damper, the interior of the baseline damper is assumed to deform as

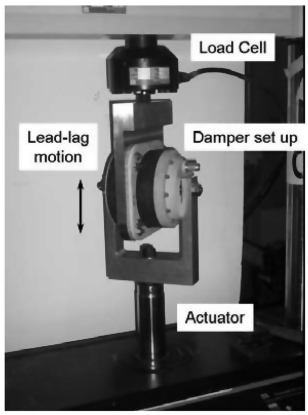

a) Fluidlastic® lag damper test set-up on MTS testing machine

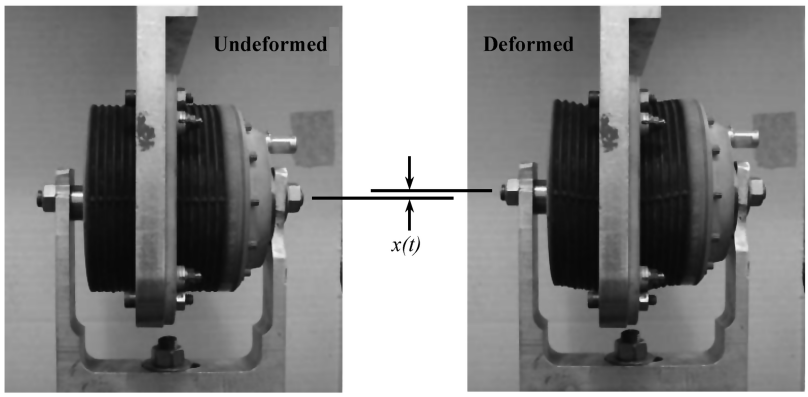

b) Deformation of Fluidlastic® lag damper on MTS testing machine

Fig. 4 Fluidlastic lag damper test setup on MTS testing machine.

shown in Figs. 4a and 4b. In the actual rotor-blade setting, the lag damper is intended to accommodate both radial and translational lead-lag motions of the blades. However, for small displacements, approximating actual lead-lag motion of the rotor blades using translational motion is assumed to be acceptable. The forcing function is applied at the damper midplate, which creates a triangular damper deformation with the upper and lower plates. This causes the volume of one of the elastomeric chambers to decrease, forcing the fluid to flow through the flow ports into the other chamber as the other chamber volume increases to compensate for the in-flow. Because of the absence of a well-defined piston and the complex damper features, the input-displacement excitation is not uniform throughout the damper height. It varies from zero at damper extremities to its maximum, which equals the input-displacement excitation, at damper center. However, all damper analysis is evaluated based on the input excitation at damper midplate.

To mimic the lead-lag motion of helicopter blades as applied to the baseline lag damper and the MRFE damper, a test fixture was fabricated to hold dampers in a 24.5 kN material testing systems (MTS) servo-hydraulic testing machine. Figures 4a and 4b show the baseline lag damper test setup, where the midplate is connected to the load cell by means of the test jig. The lower mounting bracket is attached to the lag damper through a mounting rod, which is slotted in at the mounting hole, located at the lag damper center, through the center wall. The center wall is oriented horizontally such that the motion of the MTS actuator connected to the lower bracket forces fluid to flow from one chamber to the other, by deforming the elastomeric outer wall and emulating the lead-lag motion.

The displacement and force were measured by the linear variable differential transformer (LVDT) sensor and load cell of the MTS machine. The frequencies of excitations were chosen to be 3.8 and 5.8 Hz, which correspond to an actual rotor system lag/rev frequency (i.e., the lag frequency normalized by the main rotor frequency) and 1/rev frequency (i.e., the main rotor frequency normalized in similar fashion). Three cases were studied: baseline Fluidlastic lag damper, elastomer damper body (without fluid), and the MRFE damper. For all cases, damper testing was carried out with varying excitation amplitudes. The excitation amplitudes ranged from 0.762 to 3.81 mm (30 to 150 mil) in increments of 0.50 mm (20 mil) at both lag/rev and 1/rev frequencies. For the MRFE damper, a DC power supply was employed to provide a controlled current input to the MR valve during testing. The applied current varied from 0–1 A, in increments of 0.25 A.

Figure 5 shows the force vs displacement plots at constant amplitude of the baseline Fluidlastic damper, the elastomeric body (damper body without fluid), and the MRFE damper at current values varying from 0 to 1 A. The input displacement is given by:

$$x(t) = X_s \sin(\omega t) + X_c \cos(\omega t) \tag{1}$$

The measured force data was not filtered and was used as recorded. For an amplitude of 2.286 mm, Fig. 5a shows the hysteretic behavior of both the baseline damper and elastomeric body, while Fig. 5b shows that of the MRFE damper. In each force-displacement plot, the area enclosed by the hysteresis loop is proportional to the amount of energy dissipated per cycle. The damping available is in turn proportional to the energy dissipated per cycle. Referring to Fig. 5a, it is observed that the force-displacement curves of the baseline Fluidlastic and elastomeric dampers show fixed damping. The hysteretic force-displacement curves for the Fluidlastic and elastomeric dampers are also elliptical in shape and inclined at a fairly constant angle. When a force is applied to the empty elastomeric body, the elastomer is assumed to deform in shear, and the resulting hysteresis is shown in Fig. 5a. The small enclosed area of the elastomer hysteresis indicates that, in shear mode, the elastomer contributes a small fraction of the total damping of the baseline Fluidlastic damper. The majority of the baseline damping is contributed primarily through viscous damping and secondarily through elastomer bulge damping, which will be discussed in later sections. From Fig. 5b, the MRFE damper at zero applied current behaves in a similar manner as the Fluidlastic and elastomeric dampers, having an elliptical force-displacement plot. Under the application of a magnetic field, the MRFE damper behavior transforms substantially, exhibiting significant nonlinearity. This property, demonstrated in Fig. 5b, shows the hysteretic plots of the MRFE damper under varying input currents. As control current is applied, the dissipated energy per cycle, thus the available damping in the MRFE device, increases significantly. This is due to the additional controllable damping contribution from the MR effect, on top of the viscous and bulge damping.

A typical approach for characterization of damper performance is the complex modulus method. It is a linear characterization technique of damper properties which treats the complex stiffness k^* as a combination of the in-phase stiffness k' and the loss stiffness k'', given as:

$$k^* = k' + ik'' = k'(1 + i\eta) \tag{2}$$

where the loss factor η is defined as the ratio of the loss stiffness to the in-phase stiffness. The damper force is estimated by the first Fourier sine and cosine components at the excitation frequency:

$$F(t) = F_s \sin(\omega t) + F_c \cos(\omega t) = k'x(t) + \frac{k''}{\omega}\dot{x}(t) \tag{3}$$

The in-phase stiffness k' and quadrature stiffness k'' are determined by substituting the displacement function and its derivative from Eq. (1) into the force equation:

$$k' = \frac{F_c X_c + F_s X_s}{X_c^2 + X_s^2} \tag{4}$$

$$k'' = \frac{F_c X_s - F_s X_c}{X_c^2 + X_s^2} \tag{5}$$

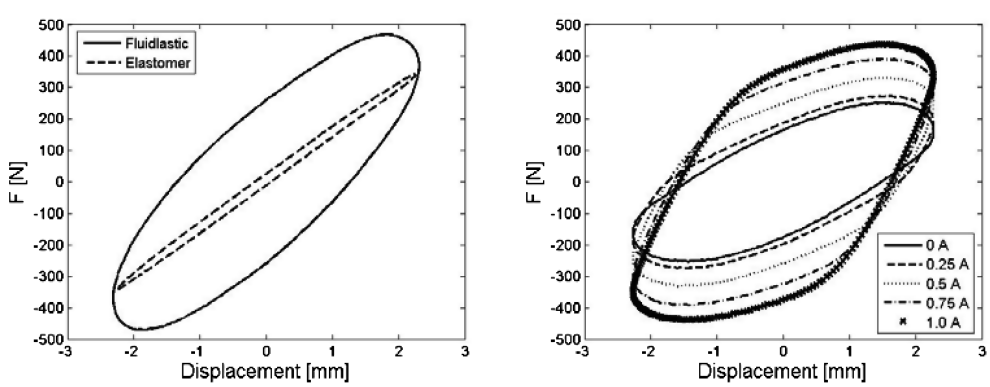

a) Fluidlastic® damper and elastomer body b) MRFE damper

Fig. 5 Typical force-displacement hysteresis results at fixed amplitude.

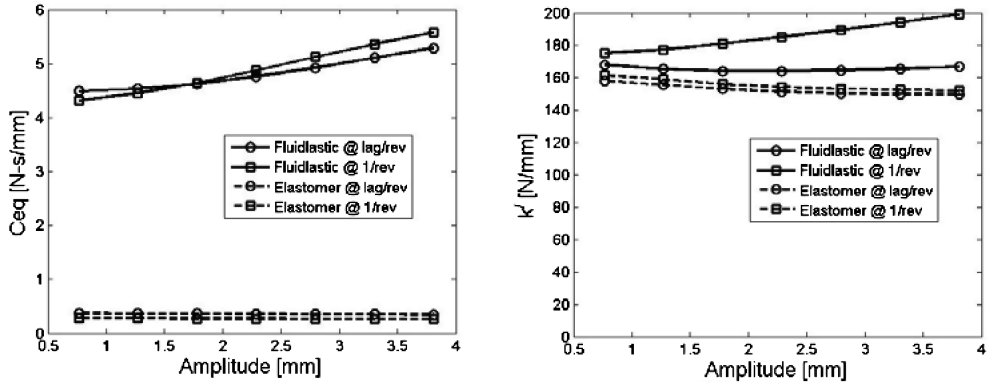

a) Equivalent damping **b) In-phase stiffness**

Fig. 6 Complex modulus characterization of Fluidlastic damper and elastomer.

The equivalent damping C_{eq} is approximated by

$$C_{eq} \cong \frac{k''}{\omega} \tag{6}$$

This linearization technique is an approximation because the complex stiffness assumes steady-state harmonics at the excitation frequency. However, it gives an acceptable representation of the linearized in-phase stiffness and equivalent damping of the elastomeric, Fluidlastic, and MRFE dampers for comparing overall damping performance under different loading conditions.

The in-phase k' stiffness and equivalent damping C_{eq} of the elastomer and the Fluidlastic dampers at lag/rev and 1/rev frequencies are shown in Fig. 6. We observe that C_{eq} of the baseline damper shows moderate amplitude dependence at both frequencies, while it remains fairly constant for the elastomer. Both the baseline and elastomer show a weak dependence on excitation frequency. Further, the majority of the energy dissipation is supplied through viscous damping and bulge damping (see Secs. IV and V), with a very small contribution from the elastomer in shear. However, this method cannot show the individual damping contributions of the viscous and compliance components, which are crucial in designing the lag damper. The in-phase stiffness also shows a fairly weak dependence on amplitude, with a maximum increment of about 12% in the case of the baseline damper at 1/rev frequency. The close correlation between stiffness of the baseline and the elastomer body indicates that a substantial amount of the Fluidlastic-damper in-phase stiffness comes from the elastomer.

The damping coefficient and loss factor of the MRFE and baseline dampers at lag and rotor frequencies are shown in Figs. 7 and 8, respectively. Figure 7a shows the equivalent damping of the Fluidlastic and MRFE dampers at the lag frequency as a function of lag motion for different constant applied currents. The dotted line in Fig. 7a is the equivalent damping of the current baseline damper. Although the viscosity of the MR fluid is lower than the silicone fluid used in the baseline damper, the passive damping component of the MRFE damper has additional viscous losses due to the retrofit components. However, the field-off (0 A) equivalent damping of the MRFE damper is still lower than that of the baseline damper, which was a goal of this design. This is beneficial for reducing helicopter hub loads since high damping is not required for most flight conditions. Comparatively, the maximum field-on (1 A) equivalent damping of the MRFE damper is higher than the baseline damper such that the required lag damping at certain flight conditions can be achieved. Notably, the equivalent damping of the MRFE damper can be varied dramatically as a function of the applied current, and the minimum damping increase can be as high as 200% at the low-amplitude lag-motion condition. This allows a large damping controllable range and thus, the ability to optimize damping at different flight conditions.

Loss factor, which is a ratio between loss stiffness and in-phase stiffness, is also a key characterization parameter to describe the behavior of a spring–mass system. Figure 7b gives the loss factor of the MRFE damper at lag frequency. The loss factor, shown as a dotted line, is obtained from the baseline Fluidlastic damper. The field-off loss factor of the MRFE damper is at least 35% higher than the baseline damper. The loss factor of the MRFE is higher than the baseline damper at all times, indicating greater available damping. As the applied current initially increases, the loss factor of the MRFE damper generally increases and then shows a reduction at lower amplitudes. The in-phase stiffness of the MRFE damper is high at low displacements and high fields, resulting in a relatively lower loss factor. Notably, the loss factor decreases with decreasing amplitude as the applied current is over 0.5 A.

Having determined that the MRFE can potentially augment damping at the design lag/rev frequency, the next set of results will compare the damping and loss factor of this damper at the primary rotor frequency of 5.8 Hz. Evaluation at 1/rev is important in the development of the MRFE damper because during high-speed

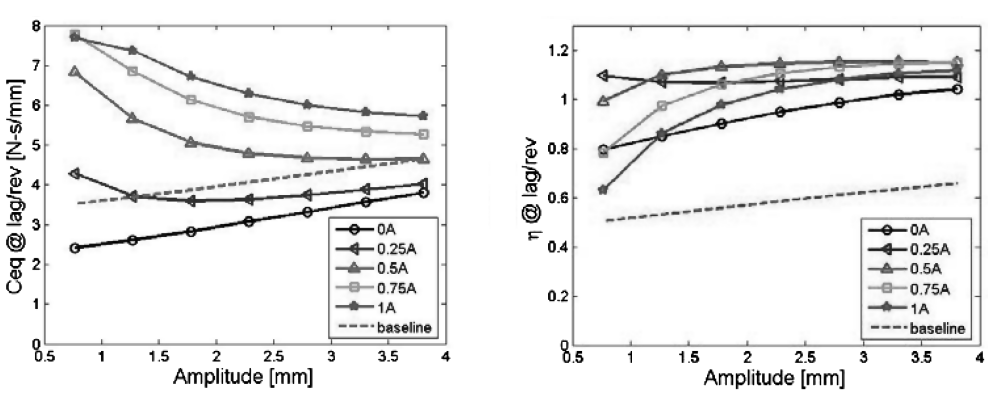

a) Equivalent damping **b) Loss factor**

Fig. 7 Complex modulus characterization of MRFE damper at lag/rev.

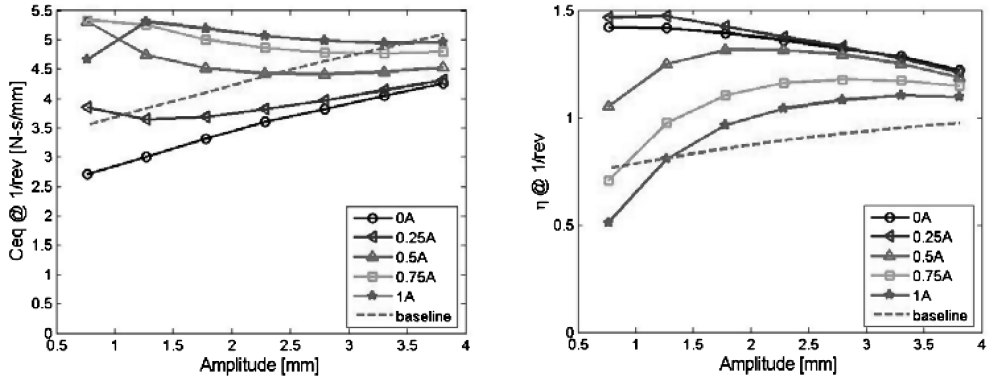

a) Equivalent damping **b) Loss factor**

Fig. 8 Complex modulus characterization of MRFE damper at 1/rev.

forward flight, the forced lag motion occurs at the 1/rev rotor frequency. Figure 8 displays these results. The equivalent damping at 1/rev resembles the response at lag/rev, in that the damping range of the MRFE device extends above and below the baseline damper performance. However, the dynamic range of the MRFE damper is observed to decrease at this frequency. It is believed that this is due to choked flow in the MR valves. During the field-on condition, as the excitation frequency rises, fluid velocity in the MR valve tends to further increase, enhancing viscous-flow effects. However, it can still be seen that the MRFE damper generally has a better loss factor than the baseline (Fig. 8b).

IV. Nonlinear hydromechanical modeling

Because of the elliptical force-displacement hysteretic behavior of the Fluidlastic, elastomeric, and MRFE damper (zero field), the linear complex modulus model (Kelvin-type model) can capture the hysteresis that these dampers exhibit. The amplitude-dependent in-phase stiffness k' and equivalent damping C_{eq} determined from the complex modulus method can be applied as the spring stiffness and damping coefficient of the Kelvin model. However, in the baseline and MRFE damper systems, this method cannot delineate the stiffness and damping contributions from the elastomer in shear, elastomer compliance, and viscous flow. In addition, under the application of a magnetic field, the MRFE damper exhibits a nonlinear behavior (Fig. 5b), and the complex modulus method cannot accurately represent this behavior. In addition, the physical-flow motion of the fluid- or hydraulic-based baseline and MRFE lag dampers is not well-represented. Thus, to describe the flow dynamics and predict the nonlinear hysteretic damping force of the MRFE damper, a hydromechanical model based on hydraulic and mechanical lumped parameters is proposed. The proposed lumped-parameter control volumes are shown in Fig. 9. For clarity, the two MR valves are identified with subscripts a and b. There are two volume chambers (1 and 5), which are lumped into pressures P_1 and P_5 and compliances S_1 and S_5. Both S_1 and S_5 represent the compliances of the fluid and the chamber. However, since the elastomeric cylinder and center wall are much more compliant than the MR fluid, they dominate the compliances of the chambers. Control volumes $a2$, $a3$, $b2$, and $b3$ are lumped into fluid inertances I_{a2}, I_{a3}, I_{b2}, and I_{b3} and passive-flow resistances R_{a2}, R_{a3}, R_{b2}, and R_{b3}. Control volumes $a4$ and $b4$ are also lumped into fluid inertances I_{a4} and I_{b4} and passive-flow resistances R_{a4} and R_{b4}, respectively, while ΔP_{a4} and ΔP_{b4} are the pressure drops due to the yield stress of the MR fluid in the corresponding control volumes. A one-dimensional fluid flow is assumed such that the velocity and pressure of a control volume are spanwise constant at a particular time, but are time varying. In addition, incompressible flow is also assumed.

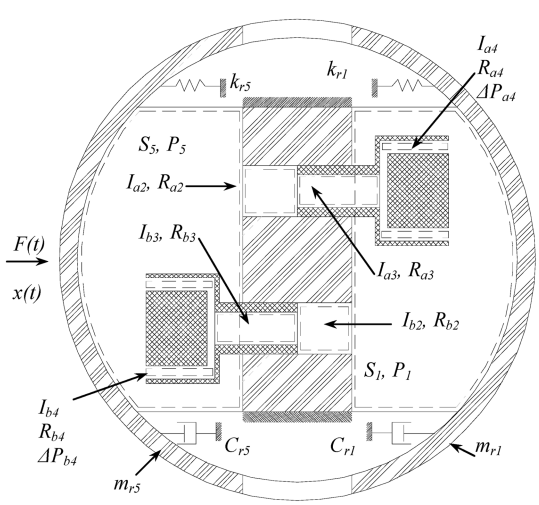

Fig. 9 Proposed hydromechanical model of MRFE damper.

The model is first formulated for a general case where the two valves and two chambers are assumed to be dissimilar. The Kelvin chain model is assumed for the elastomer shear deformation. The two elastomeric chambers are broken into two semicircular walls connected at the center, and they are assigned masses m_{r1} and m_{r5}. The shear-mode in-phase stiffness and equivalent damping of the elastomeric body from the complex modulus method are used as the spring constants k_{r1} and k_{r5} and damping coefficients C_{r1} and C_{r5}. These values were estimated by pouring out the viscous fluid from the MRFE device and testing the empty damper.

The proposed lumped parameter model includes three lumped masses (m_A, m_B, and m_r) and three dynamic degrees of freedom ($x(t)$, $x_A(t)$, and $x_B(t)$), as will be shown later. From the Kelvin model, the governing equation of motion of the elastomer is given by

$$F(t) - (k_{r1} + k_{r5})x(t) - (C_{r1} + C_{r5})\dot{x}(t) - A_p(P_5(t) - P_1(1)) = (m_{r1} + m_{r5})\ddot{x}(t) \tag{7}$$

Similar to an elastomer deformed in shear, bulging of an elastomer due to volumetric expansion exhibits damping. Colgate et al. [45] recommend that some improvement could be attained in modeling by considering bulge damping. This bulge or compliant damping is captured by introducing a resistant parameter [42] on the net flow into the compliant chambers resulting in the volumetric expansion. Thus, applying the continuity argument to the volume chambers 1 and 5 and introducing bulge resistances R_1 and R_5, the following equations are obtained:

$$A_p\dot{x}(t) - q_a(t) - q_b(t) = S_5(\dot{P}_5(t) - R_5(A_p\ddot{x}(t) - \dot{q}_a(t) - \dot{q}_b(t))) \tag{8}$$

$$-A_p\dot{x}(t) + q_a(t) + q_b(t) = S_1(\dot{P}_1(t) - R_1(-A_p\ddot{x}(t) + \dot{q}_a(t) + \dot{q}_b(t))) \tag{9}$$

where the flow rates through valve a and b in terms of inertance displacements x_{ai} and x_{bi} are given by

$$q_a(t) = A_{a2}\dot{x}_{a2}(t) = A_{a3}\dot{x}_{a3}(t) = A_{a4}\dot{x}_{a4}(t) \tag{10}$$

$$q_b(t) = A_{b2}\dot{x}_{b2}(t) = A_{b3}\dot{x}_{b3}(t) = A_{b4}\dot{x}_{b4}(t) \tag{11}$$

where A_{ai} and x_{ai} are the cross-sectional area and fluid-inertance displacement of the ith lump or control volume. The combined compliances of the fluid chambers for control volume 1 and 5 are given by

$$S_1 = \frac{A_p^2}{k_{c1}}, \qquad S_5 = \frac{A_p^2}{k_{c5}} \tag{12}$$

Here, k_{c1} and k_{c5} represent the bulge stiffness effects of the two volume chambers, which are dominated by the elastomer bulge-stiffness contribution. Because of the complexity of the damper design, deformation, and the absence of a well-defined piston, an equivalent piston area A_p is formulated to account for the total displaced fluid volume due to forced elastomer deformation.

Also, from the hydraulic model shown in Fig. 9, the total pressure drop in the two port holes (control volumes 2 and 3) and MR valve annular gap (4) due to flow of the MR fluid is given by

$$(P_5(t) - P_1(t)) = I_a\dot{q}_a(t) + R_a q_a(t) + \Delta P_{a4}(q_a(t)) \tag{13}$$

$$(P_5(t) - P_1(t)) = I_b\dot{q}_b(t) + R_b q_b(t) + \Delta P_{b4}(q_b(t)) \tag{14}$$

The terms I_a, R_a, and ΔP_a are given by

$$I_a = \rho \sum_{i=2}^{4} \frac{l_{ai}}{A_{ai}} \tag{15}$$

$$R_a = \frac{128\mu_o}{\pi}\sum_{i=2}^{3}\left(\frac{l_i}{D_i^4}\right)_a + 12\mu_{\mathrm{MR}}\left(\frac{l_4}{A_d d_4^2}\right)_a + R_{\text{min or losses}} \tag{16}$$

$$\Delta P_{a4} = 2\frac{l_{a4}}{d_{a4}}\tau_{ya}(H) \tag{17}$$

Under the Bingham assumption, the fluid viscosity and the postyield viscosity are assumed equal ($\mu_o = \mu_{\mathrm{MR}}$). The yield stress of the MR fluid at the applied magnetic field is represented by $\tau_y(H)$. The term ΔP can be interpreted as the minimum required differential pressure below which flow is fully restricted. The equation for the resistance is derived from laminar-flow analysis. The above equations also hold true for the second flow path by replacing the subscript a with b. Because of laminar-flow assumption with low Reynolds number, the minor losses are neglected.

By eliminating the internal variables P_1 and P_5 from Eqs. (7–9), (13), and (14), we obtain the following two equations of motion in terms of time varying variables $x(t)$ and $x_A(t)$:

$$\begin{aligned}&(m_{r1} + m_{r5})\ddot{x}(t) + (C_{r1} + C_{r2})\dot{x}(t) + (k_{r1} + k_{r2})x(t)\\ &\quad + (C_{c1} + C_{c5})(\dot{x}(t) - (1+\psi)\dot{x}_A(t)) + (k_{c1} + k_{c5})(x(t)\\ &\quad - (1+\psi)x_A(t)) = F(t)\end{aligned} \tag{18}$$

$$\begin{aligned}&m_A\ddot{x}_A(t) + C_A\dot{x}_A(t) - (C_{c1} + C_{c5})(\dot{x}(t) - (1+\psi)\dot{x}_A(t))\\ &\quad - (k_{c1} + k_{c5})(x(t) - (1+\psi)x_A(t)) + F_{yA}\mathrm{sgn}(\dot{x}_A(t)) = 0\end{aligned} \tag{19}$$

The valve factor ψ is given by

$$\psi(i\omega) = \frac{x_A}{x_B}(i\omega) = \frac{(m_B - \frac{F_{yA}-F_{yB}}{\omega^2 x_B(i\omega)})i\omega + C_B}{m_A i\omega + C_A} \tag{20}$$

The terms x_A, m_A, C_A, and F_{yA} for valve A and bulge damping C_{c1} and C_{c5} are expressed as

$$\begin{aligned}&x_A = (A_{a4}/A_p)x_{a4}, \qquad m_A = I_a A_p^2 \qquad C_A = R_a A_p^2\\ &F_{yA} = \Delta P_{a4}A_p \qquad C_{c1} = R_1 A_p^2, \qquad C_{c5} = R_5 A_p^2\end{aligned} \tag{21}$$

Replacing subscripts A and a with B and b in the above equations will give the corresponding terms for the second flow valve. Here, F_{yA} and F_{yB} represent the controllable yield forces in each MR valve and are a function of the applied magnetic field. The valve factor ψ, which relates the generalized inertance variables x_A and x_B, varies from zero (no flow in valve b) to infinity (no flow in valve a). The valve factor is a function of the head losses encountered in the MR valves as shown in Eq. (20). Bulge damping C_{c1} and C_{c5} represent the damping contribution of the elastomeric body due to volumetric flexing of fluid chambers.

Figure 10 gives the mechanism of the proposed hydraulic model, which is composed of parallel and series combinations of linear springs, dashpots, and Coulomb friction elements. The analogous mechanical system (Fig. 10) and governing equations (18–20) show that, in the preyield region, the hysteresis behavior is evident in the chamber compliance effects ($C_{c1}, C_{c5}, k_{c1}, k_{c5}$). The Coulomb elements (F_{yA}, F_{yB}), generalized inertance masses (m_A, m_B), and

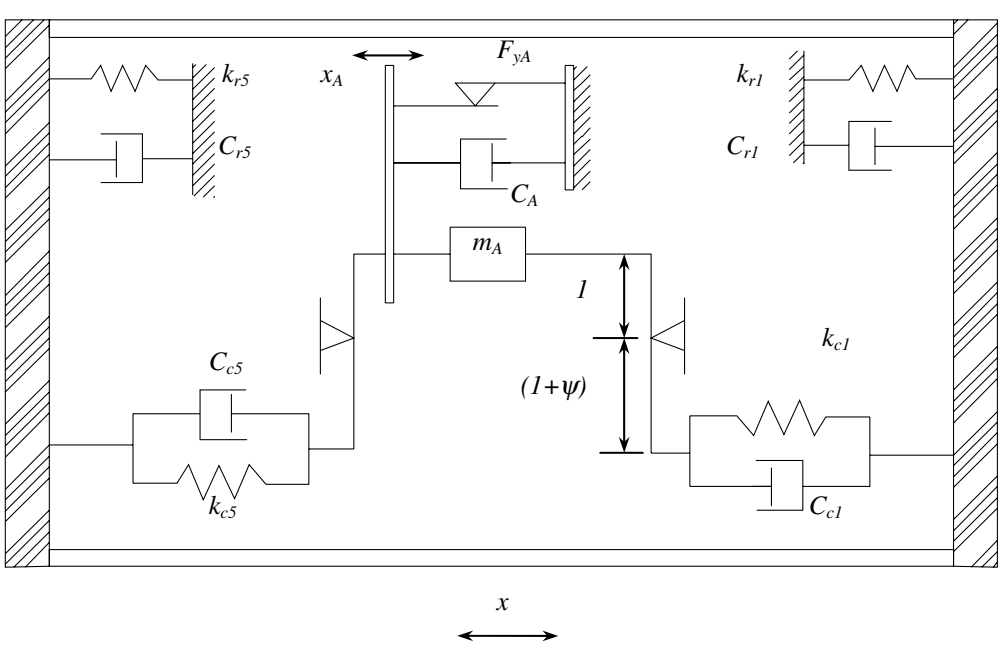

Fig. 10 Analogous mechanical system of the hydromechanical model of the MRFE damper.

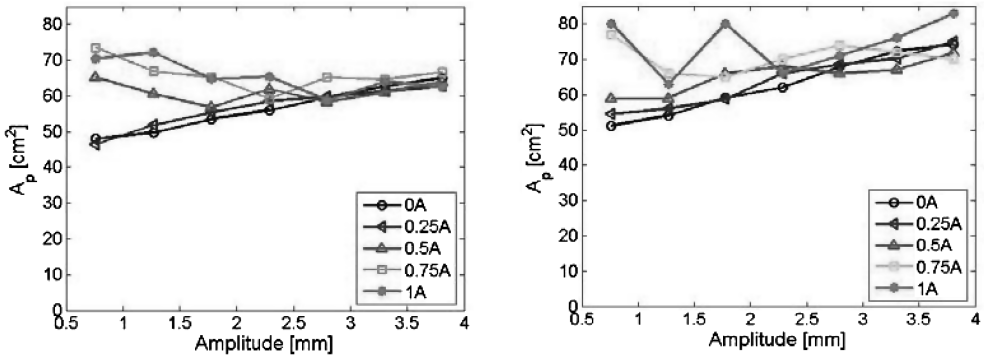

a) Equivalent area at lag/rev, A_p b) Equivalent area at 1/rev, A_p

Fig. 11 Optimized equivalent piston area A_p.

viscous damping terms (C_A, C_B) represent the postyield behavior. It is observed that the flow motion and coupling of the mechanical and hydraulic systems of the MRFE damper is illustrated well by governing equations.

In our present design, since there are two identical MR valves and elastomeric chambers, the following assumptions will hold true: $F_{yA} = F_{yB} = F_y$, $k_{c1} = k_{c5} = k_c$, $C_{c1} = C_{c5} = C_c$, $m_{r1} = m_{r5} = m_r$, $k_{r1} = k_{r5} = k_r$, $C_{r1} = C_{r5} = C_r$, and $\psi = 1$. Thus, the equations of motion from Eqs. (18–20) will further reduce to

$$2m_r\ddot{x}(t) + 2C_r\dot{x}(t) + 2k_r x(t) + 2C_c(\dot{x}(t) - 2\dot{x}_A(t)) + 2k_c(x(t) - 2x_A(t)) = F(t) \tag{22}$$

$$m_A\ddot{x}_A(t) + C_A\dot{x}_A(t) - 2C_c(\dot{x}(t) - 2\dot{x}_A(t)) - 2k_c(x(t) - 2x_A(t)) + F_{yA}\mathrm{sgn}(\dot{x}_A(t)) = 0 \tag{23}$$

V. Parameter identification and model validation

To begin the optimization procedure to accurately simulate measured damper dynamics, some parameters were estimated a priori to lower the number of optimized parameters. The viscosity and density of the MR fluid is known, so that the fluid resistance and inertance values can be estimated using Eqs. (15) and (16). These values remain constant since they are not a function of input displacement and applied current. The shear stiffness and damping of the elastomer are also estimated from measurements (Figs. 5 and 6). To minimize the mean squared error between the measured and predicted damping force of the MRFE damper, a constrained least-mean-squared (LMS) error minimization technique was employed to estimate and optimize the equivalent piston area A_p, bulge stiffness k_c, bulge damping C_c, and yield force F_y. The rubber mass is neglected in this optimization. The error function for the hydro-mechanical model is expressed as

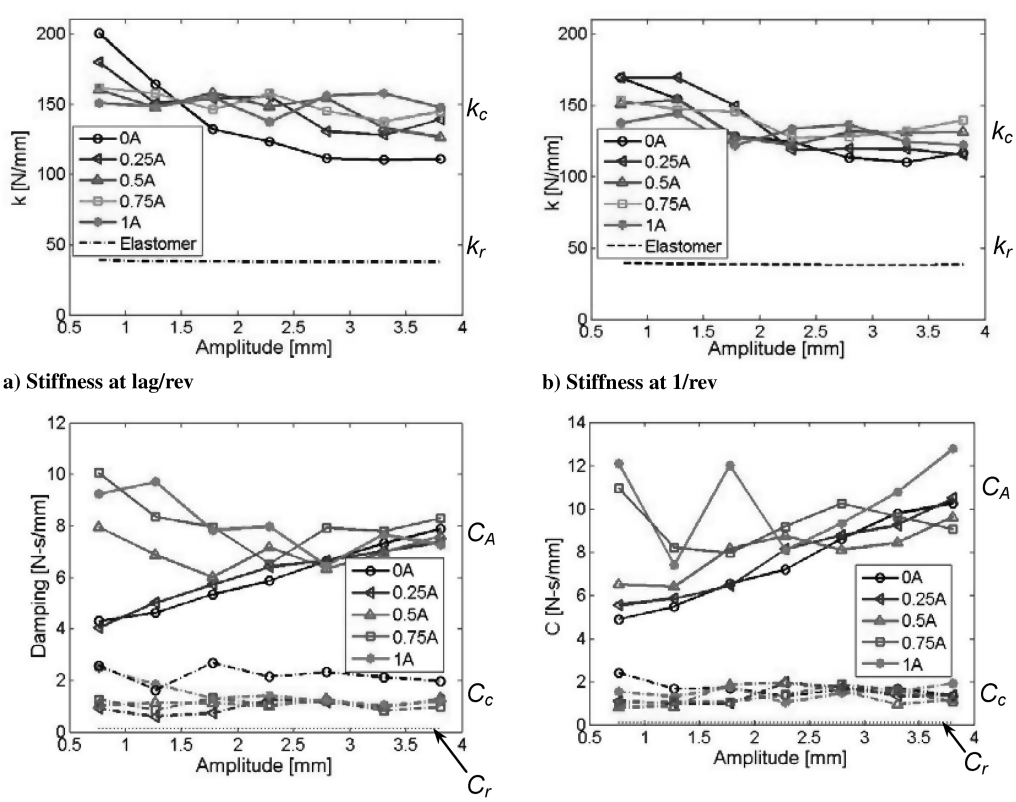

a) Stiffness at lag/rev b) Stiffness at 1/rev

c) Damping at lag/rev d) Damping at 1/rev

Fig. 12 Stiffness and damping contribution of MRFE components.

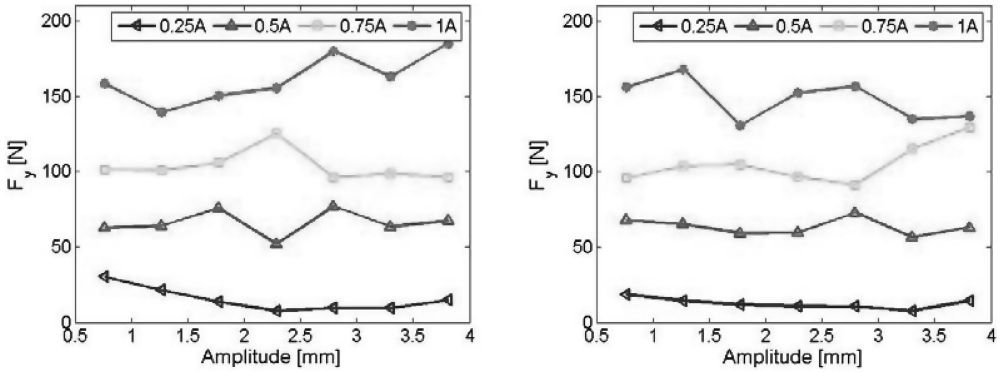

a) Yield force at lag/rev, F_y b) Yield force at 1/rev, F_y

Fig. 13 Optimized yield force F_y.

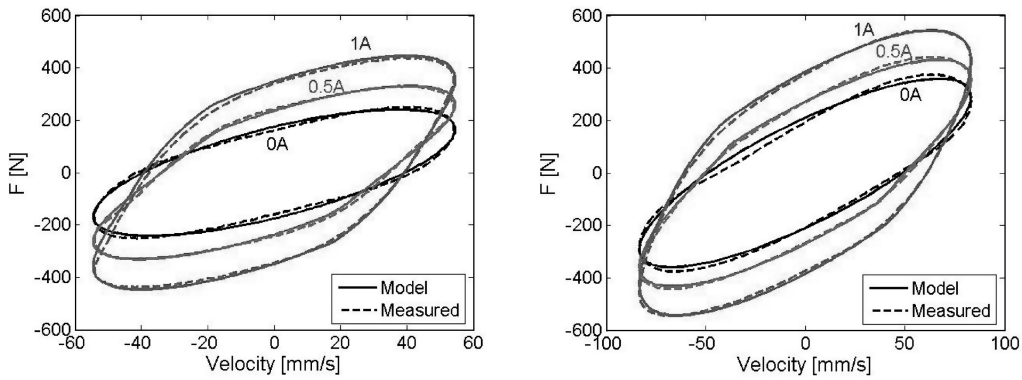

a) Model performance at lag/rev b) Model performance at 1/rev

Fig. 14 Experimental and model-estimated damping force hysteresis.

$$E(A_p, k_c, C_c, F_y) = \sum_{j=1}^{n} (F(t_j) - F^*(t_j))^2 \tag{24}$$

Figures 11a and 11b show the optimized equivalent piston areas obtained from the error minimization procedure at different amplitudes and frequencies. The shear stiffness and bulge stiffness of the MRFE damper at lag/rev and 1/rev are given in Figs. 12a and 12b respectively. The damping contributions from the hydraulic and mechanical components are given in Figs. 12c and 12d. The plots show that the majority of the MRFE device passive damping is provided through viscous damping, while elastomeric shear deformation contributes minimal damping. Figure 13 shows the variation of yield force F_y as obtained from model optimization. The yield force increases with increasing applied current, and this trend is similar at both frequencies.

The damping force versus velocity cycles at lag/rev and 1/rev frequencies and different applied fields are given in Fig. 14. Figure 14a shows the force–velocity hysteresis plots at lag/rev frequency, and Fig. 14b shows the plots at 1/rev. The displacement amplitude for each case is 2.286 mm. The figures show that the hydromechanical model is able to capture the nonlinear dynamic behavior and closely estimates the actual hysteretic damping force behavior of the MRFE damper from experimental measurements.

The hydromechanical model is formulated on the basis that it can describe or estimate the physical-flow phenomenon that is inherent to the MRFE damper system. Based on this assumption, the MR effect contributed to the damper system is extracted from the model. At both frequencies, the input amplitude was chosen to be 2.286 mm (0.09 in) while the current is varied from 0, 0.5, and 1 A. The MR effect in each valve of the damper system, as extracted from the model [Eq. (23)], is given by

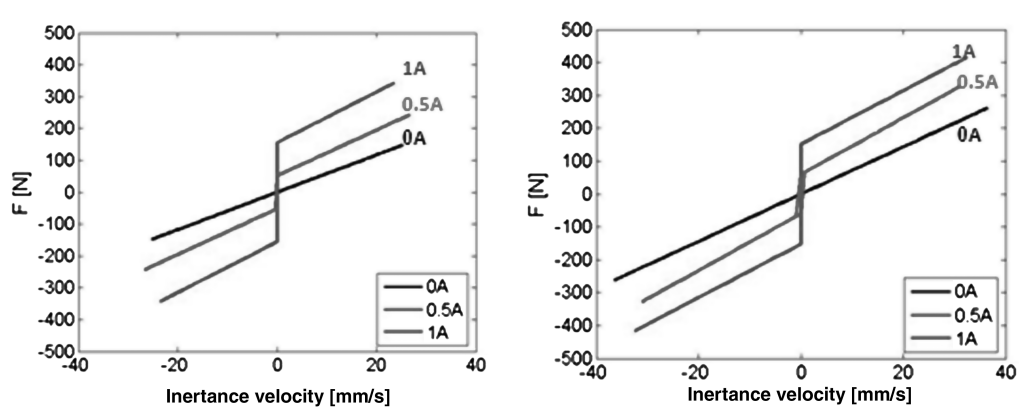

a) Lag/rev F_{MR} vs generalized inertance velocity b) 1/rev F_{MR} vs generalized inertance velocity

Fig. 15 Model-estimated MR valve damping force hysteresis at lag/rev.

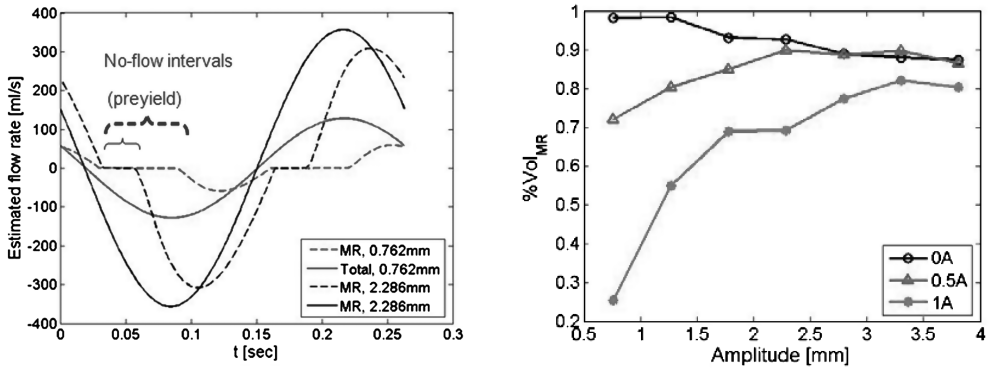

a) Total and valve flow rates at I = 1A, X_{lag} = 2.286 mm and X_{lag} = 0.762 mm

b) Half cycle volume flow through MR valve: $\%\mathrm{Vol}_{MR}$

Fig. 16 Total and MR valve flow-rate comparisons at lag/rev.

$$F_{\mathrm{MR}}(t) = C_A\dot{x}_A(t) + F_{ya}(\dot{x}_A(t)) \tag{25}$$

The first term in the above equation is related to the viscous effect, and the second Coulomb term results from the magnetic effect. These results are shown in Fig. 15. The model is able to show the Bingham-type flow typical of MR fluids, with the y-intercept of the force–velocity plot reflecting the yield force of the MR fluid. It is shown that the active damping of the MRFE is contributed by the MR effect activated through the applied current. As the applied current is increased, the yield force increases, and thus damping is increased.

Further, the total flow rate $A_p\dot{x}(t)$ and flow rate through MR valves $2A_p\dot{x}_A(t)$ at lag/rev frequency were plotted and compared at the field-on condition ($I = 1$ A) at two different input amplitudes. As shown in Fig. 16a, the MR valve flow rate is less than the total. This is manifested in the no-flow interval region in the figure. At this condition, the MR fluid has not yet yielded, and volume compensation is attained through bulging of the elastomeric damper body. In addition, as the input amplitude increases, more of the total fluid flow goes through the valves. This is because the MR fluid yields faster at higher velocity, giving the fluid more time to flow through the valves. The portion of the total displaced volume per half cycle that flows through the MR valve ($\%\mathrm{Vol}_{\mathrm{MR}}$) is estimated from the formulated model per the following equation:

$$\%\mathrm{Vol}_{\mathrm{MR}} = \left.\frac{\int 2A_p\dot{x}_A(t)\mathrm{d}t}{\int A_p\dot{x}(t)\mathrm{d}t}\right|_{\mathrm{halfcycle}} * 100\% \tag{26}$$

These results are shown in Fig. 16b. The plots show that, at the field-on condition, $\%\mathrm{Vol}_{\mathrm{MR}}$ increases with increasing amplitude. In addition, as the applied current is increased, $\%\mathrm{Vol}_{\mathrm{MR}}$ decreases due to the increased MR effects.

To predict the response of the MRFE damper under dual-frequency excitation, it was subjected to various combinations of lag/rev and 1/rev frequency amplitudes under various applied currents, and the force time history is used to evaluate the model performance. Using optimized model parameters, the MRFE damper

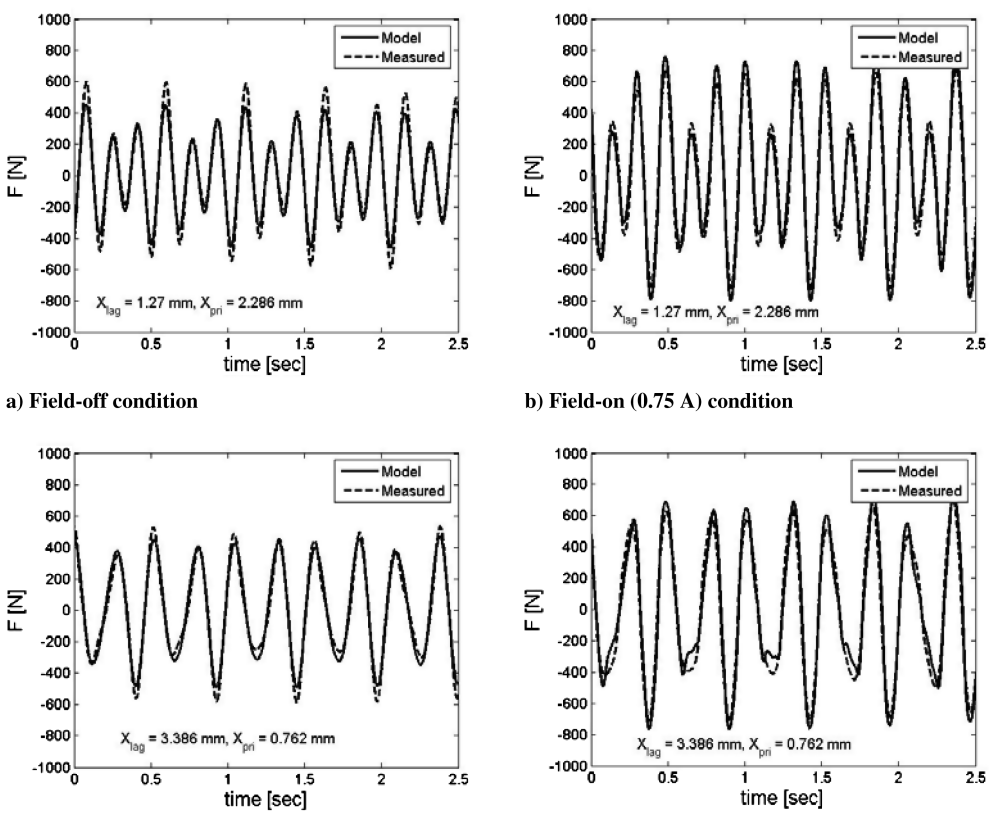

a) Field-off condition

b) Field-on (0.75 A) condition

c) Field-off condition

d) Field-on (0.75 A) condition

Fig. 17 Dual-frequency experimental and model-estimated damping forces comparison.

dual-frequency response was predicted by linear superposition of the estimated damper performance at each excitation frequency. The modeling results for a combination of the lag/rev and 1/rev frequencies at field-off and field-on conditions are given in Fig. 17. The results show that the hydromechanical model was able to predict MRFE damper dual-frequency performance reasonably well over the amplitudes and frequencies investigated.

VI. Conclusions

Hingeless and bearingless helicopters are equipped with lag dampers to mitigate instabilities such as air and ground resonance. Currently, most bearingless helicopters use either elastomeric or hybrid fluid–elastomeric dampers. However, elastomeric lag dampers exhibit strong amplitude- and frequency-dependent damping and stiffness losses. In addition, both elastomeric and fluid–elastomeric or Fluidlastic are adversely affected by temperature. Unlike these passive dampers, an MRFE lag damper has the potential to compensate for damping losses due to inherent material properties or extreme environmental conditions by the application of a controllable magnetic field. The MRFE damper was investigated to establish its potential in augmenting damping during flight conditions in which instabilities are likely to occur, and in compensating for adverse environmental conditions.

To this effect, a snubber-type Fluidlastic lag damper was retrofitted to develop an MRFE lag damper. The MRFE design does not introduce any moving parts to the system in an effort to preserve the proven reliability and maintenance-free conditions of the original baseline damper. This investigation demonstrated the feasibility of using the MRFE damper to mitigate helicopter rotor instabilities with fixed-frame experiments. The MRFE damper can provide comparable damping force to the baseline snubber damper. Moreover, a substantial increase in damping and a wide controllability range can be gained by using the MRFE damper. Up to a 200% change in damping was obtained over the amplitude range tested. This damping and controllability range of the MRFE damper can be tuned to match actual damping requirements of certain flight conditions in which stability margins may deteriorate. Designing the device with reduced field-off damping helps decrease rotor-hub loading because higher damping is only required at specific flight conditions. In addition, pairs of MRFE dampers can be tuned to match one another, thus, enhancing rotor-blade tracking.

To account for the nonlinear behavior of the MRFE damper, a lumped-parameter-based, hydromechanical model was formulated and validated. The model describes the interaction of the mechanical, hydraulic, and magnetorheological phenomena within the damper system. The hydromechanical model is a semi-empirical model in which parameters are fundamentally dependent on damper geometry and material properties at a given test condition. Thus, physical parameters like fluid inertance and resistance, chamber compliance, and yield force are considered. This model was shown to accurately estimate the field-dependent hysteretic damping force and illustrate the physical-flow motion of the MRFE damper, making it valuable for future design and feedback-control studies.

Acknowledgements

This work was supported by a DARPA Phase II SBIR project, contract number W31P4Q06C0400, with technical monitor Daniel Newman. Approved for public release, distribution unlimited. Technical guidance from LORD Corp. on MR Fluid and damper details is gratefully acknowledged. The first author would also like to acknowledge fellowship support from the Alfred P. Sloan Foundation.

References

[1] Chopra, I., "Perspective in Aeromechanical Stability of Helicopter Rotors," *Vertica*, Vol. 14, No. 4, 1990, pp. 457–508.

[2] Jones, P., Russell, D., and McGuire, P., "Latest Development in Fluidlastic Lead-Lag Dampers for Vibration Control in Helicopters," *59th Annual Forum Proceedings*, AHS International, Alexandria, VA, 2003, pp. 566–575.

[3] Grilli, R., Krishnan, R., Wereley, N. M., and Sieg, T., "Mechanisms-Based Analysis of Filled Elastomeric Dampers Under Single and Dual Frequency Excitations," *Journal of the American Helicopter Society*, Vol. 53, No. 3, 2008, pp. 252–266. doi:10.4050/JAHS.53.252

[4] Panda, B., Mychalowycz, E., and Tarzanin, F., "Application of Passive Dampers to Modern Helicopters," *Smart Materials and Structures*, Vol. 5, No. 5, 1996, pp. 509–516. doi:10.1088/0964-1726/5/5/001

[5] Hu, W., and Wereley, N. M., "Distributed Rate-Dependent Elastoslide Model for Elastomeric Lag Dampers," *Journal of Aircraft*, Vol. 44, No. 6, 2007, pp. 1972–1984. doi:10.2514/1.26409

[6] Felker, F., Lau, B., McLaughlin, S., and Johnson, W., "Nonlinear Behavior of an Elastomeric Lag Damper Undergoing Dual-Frequency Motion and its Effect on Rotor Dynamics," *Journal of the American Helicopter Society*, Vol. 32, No. 4, 1987, pp. 45–53. doi:10.4050/JAHS.32.45

[7] Hu, W., and Wereley, N. M., "Hybrid Magnetorheological Fluid–Elastomeric Lag Dampers for Helicopter Stability Augmentation," *Smart Materials and Structures*, Vol. 17, No. 4, 2008, p. 045021. doi:10.1088/0964-1726/17/4/045021

[8] McGuire, D. P., "Fluidlastic Dampers and Isolators for Vibration Control in Helicopters," *50th Annual Forum Proceedings*, Vol. 1, American Helicopter Society, Alexandria, VA, 1994, pp. 295–305.

[9] Panda, B., and Mychalowycz, E., "Aeroelastic Stability Wind Tunnel Testing with Analytical Correlation of the Comanche Bearingless Main Rotor," *Journal of the American Helicopter Society*, Vol. 42, No. 3, 1997, pp. 207–217. doi:10.4050/JAHS.42.207

[10] Kamath, G. M., Wereley, N. M., and Jolly, M. R., "Characterization of Magnetorheological Helicopter Lag Dampers," *Journal of the American Helicopter Society*, Vol. 44, No. 3, 1999, pp. 234–248. doi:10.4050/JAHS.44.234

[11] Hausmann, G., and Gergely, P., "Approximate Methods for Thermoviscoelastic Characterization and Analysis of Elastomeric Lead-lag Dampers," *Proceedings of the 18th European Rotorcraft Forum*, Aeronautique et Astronautique de France, Marseille, France, 1992.

[12] Brackbill, R., Lesieutre, G., Smith, E., and Govindswamy, K., "Thermomechanical Modeling of Elastomeric Materials," *Smart Materials and Structures*, Vol. 5, 5, 1996, pp. 529–539. doi:10.1088/0964-1726/5/5/003

[13] Jolly, M., Bender, J., and Carlson, J., "Properties and Applications of Commercial Magnetorheological Fluids," *Journal of Intelligent Material Systems and Structures*, Vol. 10, No. 1, 1999, pp. 5–13. doi:10.1177/1045389X9901000102

[14] Ngatu, G., and Wereley, N. M., "High Versus Low Field Viscometric Characterization of Bidisperse MR Fluids," *International Journal of Modern Physics B*, Vol. 21, Nos. 28–29, 2007, pp. 4922–4928. doi:10.1142/S0217979207045840

[15] Genc, S., and Phule, P., "Rheological Properties of Magnetorheological Fluids," *Smart Materials and Structures*, Vol. 11, No. 1, 2002, pp. 140–146. doi:10.1088/0964-1726/11/1/316

[16] Ginder, J., and Davis, L., "Shear Stress in Magnetorheological Fluids: Role of Magnetic Saturation," *Applied Physics Letters*, Vol. 65, No. 26, 1994, pp. 3410–3412. doi:10.1063/1.112408

[17] Choi, Y. T., Wereley, N. M., and Jeon, Y. S., "Semi-active Vibration Isolation Using Magnetorheological Isolators," *Journal of Aircraft*, Vol. 42, No. 5, 2005, pp. 1244–1251. doi:10.2514/1.7919

[18] Carlson, J., "Critical Factors for MR Fluids in Vehicle Systems," *International Journal of Vehicle Design*, Vol. 33, Nos. 1–3, 2003, pp. 207–217. doi:10.1504/IJVD.2003.003572

[19] Sahin, H., Liu, Y., Wang, X., Gordaninejad, F., Evrensel, C., and Fuchs, A., "Full-scale Magnetorheological Fluid Dampers for Heavy Vehicle Rollover," *Journal of Intelligent Material Systems and Structures*, Vol. 18, No. 12, 2007, pp. 1161–1167. doi:10.1177/1045389X07083137

[20] Choi, Y. T., and Wereley, N. M., "Vibration Control of a Landing Gear System Featuring Electrorheological/Magnetorheological Fluids," *Journal of Aircraft*, Vol. 40, No. 3, 2003, pp. 432–439. doi:10.2514/2.3138

[21] Batterbee, D. C., Sims, N. D., Stanway, R., and Wolejsza, Z., "Magnetorheological Landing Gear: 1. A Design Methodology," *Smart Materials and Structures*, Vol. 16, No. 6, 2007, pp. 2429–2440.

doi:10.1088/0964-1726/16/6/046

[22] Batterbee, D. C., Sims, N. D., Stanway, R., and Rennison, M., "Magnetorheological Landing Gear: 2. Validation Using Experimental Data," *Smart Materials and Structures*, Vol. 16, No. 6, 2007, pp. 2441–2452.
doi:10.1088/0964-1726/16/6/047

[23] McManus, S. J., Clair, K. A., Boileau, P. E., Boutin, J., and Rakheja, S., "Evaluation of Vibration and Shock Attenuation Performance of a Suspension Seat with a Semi-active Magnetorheological Fluid Damper," *Journal of Sound and Vibration*, Vol. 253, No. 1, 2002, pp. 313–327.
doi:10.1006/jsvi.2001.4262

[24] Choi, S. B., Nam, M. H., and Lee, B. K., "Vibration Control of a MR Seat Damper for Commercial Vehicles," *Journal of Intelligent Material Systems and Structures*, Vol. 11, No. 12, 2000, pp. 936–944.
doi:10.1106/AERG-3QKV-31V8-F250

[25] Hiemenz, G. J., Hu, W., and Wereley, N. M., "Semi-active Magnetorheological Helicopter Crew Seat Suspension for Vibration Isolation," *Journal of Aircraft*, Vol. 45, No. 3, 2008, pp. 945–953.
doi:10.2514/1.32736

[26] Choi, Y. T., and Wereley, N. M., "Mitigation of Biodynamic Response to Vibratory and Blast-induced Shock Loads Using Magnetorheological Seat Suspensions," *Journal of Automobile Engineering*, Vol. 219, No. 6, 2005, pp. 741–754.
doi:10.1243/095440705X28330

[27] Hiemenz, G. J., Choi, Y. T., and Wereley, N. M., "Semi-active Control of a Vertical Stroking Helicopter Crew Seat for Enhanced Crashworthiness," *Journal of Aircraft*, Vol. 44, No. 3, 2007, pp. 1031–1034.
doi:10.2514/1.26492

[28] Marathe, S., Gandhi, F., and Wang, K. W., "Helicopter Blade Response and Aeromechanical Stability with a Magnetorheological Fluid Based Lag Damper," *Journal of Intelligent Material Systems and Structures*, Vol. 9, No. 4, 1998, pp. 272–282.
doi:10.1177/1045389X9800900405

[29] Zhao, Y. S., Choi, Y. T., and Wereley, N. M., "Semi-active Damping of Ground Resonance in Helicopters Using Magnetorheological Dampers," *Journal of the American Helicopter Society*, Vol. 49, No. 4, 2004, pp. 468–482.
doi:10.4050/JAHS.49.468

[30] Hu, W., Wereley, N. M., Chemouni, L., and Chen, P. C., "Semi-active Linear Stroke Magnetorheological Fluid–Elastic (MRFE) Damper for Helicopter Main Rotor Blades," *Journal of Guidance, Control, and Dynamics*, Vol. 30, No. 2, 2007, pp. 565–575.
doi:10.2514/1.24033

[31] Kamath, G., Wereley, N., and Madhavan, V., "Hysteresis Modeling of Semi-Active Magnetorheological Helicopter Dampers," *Journal of Intelligent Material Systems and Structures*, Vol. 10, No. 8, 1999, pp. 624–633.
doi:10.1106/NHLE-FNDL-U243-L8U0

[32] Panda, B., and Mychalowycz, E., "Aeroelastic Stability Wind Tunnel Testing with Analytical Correlation of the Comanche Bearingless Main Rotor," *Journal of the American Helicopter Society*, Vol. 42, No. 3, 1997, pp. 207–217.
doi:10.4050/JAHS.42.207

[33] Kunz, D., "Influence of Elastomeric Damper Modeling on the Dynamic Response of Helicopter Rotors," *AIAA Journal*, Vol. 35, No. 2, 1997, pp. 349–354.
doi:10.2514/2.100

[34] Gandhi, F., and Chopra, I., "Analysis of Bearingless Main Rotor Dynamics with the Inclusion of an Improved Time-domain Non-linear Elastomeric Damper Model," *Journal of the American Helicopter Society*, Vol. 41, No. 3, 1996, pp. 267–277.
doi:10.4050/JAHS.41.267

[35] Brackbill, C. R., Smith, E. C., Ruhl, L. E., and Lesieutre, G. A., "Characterization and Modeling of the Low Strain Amplitude and Frequency Dependent Behavior of Elastomeric Damper Materials," *Journal of the American Helicopter Society*, Vol. 45, No. 1, 2000, pp. 34–42.
doi:10.4050/JAHS.45.34

[36] Kamath, G., Hurt, M., and Wereley, N., "Analysis and Testing of Bingham Plastic Behavior in Semi-Active Electrorheological Fluid Dampers," *Smart Materials and Structures*, Vol. 5, No. 5, 1996, pp. 576–590.
doi:10.1088/0964-1726/5/5/007

[37] Wereley, N., "Non-Dimensional Herschel–Bulkley Analysis of Magnetorheological and Electrorheological Dampers," *Journal of Intelligent Material Systems and Structures*, Vol. 19, No. 3, 2008, pp. 257–268.
doi:10.1177/1045389X07088107

[38] Pang, L., Kamath, G., and Wereley, N. M., "Idealized Hysteresis Modeling of Electrorheological and Magnetorheological Dampers," *Journal of Intelligent Material Systems and Structures*, Vol. 9, No. 8, 1998, pp. 642–649.
doi:10.1177/1045389X9800900810

[39] Spencer, B., Dyke, B., Sain, M., and Carlson, J., "Phenomenological Model of a Magnetorheological Damper," *Journal of Engineering Mechanics*, Vol. 123, No. 3, 1997, pp. 230–238.
doi:10.1061/(ASCE)0733-9399(1997)123:3(230)

[40] Hu, W., and Wereley, N., "Rate-Dependent Elasto-Slide Model for Single and Dual Frequency MR Lag Damper Behavior," *International Journal of Modern Physics B*, Vol. 19, Nos. 7–9, 2005, pp. 1527–1533.
doi:10.1142/S0217979205030542

[41] Singh, R., Kim, G., and Ravindra, P. V., "Linear Analysis of Automotive Hydro-Mechanical Mount with Emphasis on De-coupler Characteristics," *Journal of Sound and Vibration*, Vol. 158, No. 2, 1992, pp. 219–243.
doi:10.1016/0022-460X(92)90047-2

[42] Geisberger, A., Khajepour, A., and Golnaraghi, F., "Non-linear Modelling of Hydraulic Mounts: Theory and Experiment," *Journal of Sound and Vibration*, Vol. 249, No. 2, 2002, pp. 371–397.
doi:10.1006/jsvi.2001.3860

[43] Hong, S. R., Choi, S. B., Choi, Y. T., and Wereley, N. M., "A Hydro-mechanical Model for Hysteretic Damping Force Prediction of ER Damper: Experimental Verification," *Journal of Sound and Vibration*, Vol. 285, Nos. 4–5, 2005, pp. 1180–1188.
doi:10.1016/j.jsv.2004.10.031

[44] Hong, S. R., Wang, G., Hu, W., and Wereley, N. M., "Hydro-mechanical Analysis of a Magnetorheological Bypass Damper," *Proceedings of the 10th International Conference on Electrorheological Fluids and Magnetorheological Suspensions*, World Scientific Publishing Company, Singapore, 2007, pp. 438–444.

[45] Colgate, J., Chang, T., Chiou, C., Liu, K., and Kerr, M., "Modeling of a Hydraulic Engine Mount Focusing on Response to Sinusoidal and Composite Excitations," *Journal of Sound and Vibration*, Vol. 184, No. 3, 1995, pp. 503–528.
doi:10.1006/jsvi.1995.0330

F. Pai
Associate Editor